

High Magnetic Field Magneto-optics on Plasmonic Silica-Embedded Silver Nanoparticles

Published as part of *The Journal of Physical Chemistry virtual special issue "Marie-Paule Pileni Festschrift"*.

Alessio Gabbani, Giulio Campo, Valentina Bonanni, Peter van Rhee, Gregorio Bottaro, César de Julián Fernández, Valentina Bello, Elvira Fantechi, Francesco Biccari, Massimo Gurioli, Lidia Armelao, Claudio Sangregorio, Giovanni Mattei, Peter Christianen, and Francesco Pineider*



Cite This: *J. Phys. Chem. C* 2022, 126, 1939–1945



Read Online

ACCESS |



Metrics & More

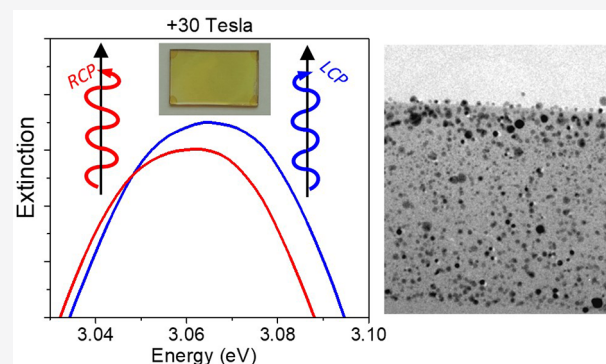


Article Recommendations



Supporting Information

ABSTRACT: Tuning the plasmonic response with an external magnetic field is extremely promising to achieve active magneto-plasmonic devices, such as next generation refractometric sensors or tunable optical components. Noble metal nanostructures represent an ideal platform for studying and modeling magnetoplasmonic effects through the interaction of free electrons with external magnetic fields, even though their response is relatively low at the magnetic field intensities commonly applied in standard magneto-optical spectroscopies. Here we demonstrate a large magnetoplasmonic response of silver nanoparticles by performing magnetic circular dichroism spectroscopy at high magnetic fields, revealing a linear response to the magnetic field up to 30 T. The exploitation of such high fields allowed us to probe directly the field-induced splitting of circular plasmonic modes by performing absorption spectra with static circular polarizations, giving direct experimental evidence that the magneto-optical activity of plasmonic nanoparticles arises from the energy shift of field-split circular magnetoplasmonic modes.



INTRODUCTION

Modulating the plasmonic resonance with an external tool can boost the performance of plasmon-based sensors and devices, enriching the tunability of light–matter interaction and enabling the detection of ultras-small changes occurring near the surface of the plasmonic nanostructures.^{1,2} To this aim, the use of external magnetic fields is extremely promising.³ Indeed, compared to other external stimuli that can be applied to control the plasmonic response, such as all-optical control,^{4–6} temperature,⁷ or electric fields,^{8,9} the action of magnetic fields on free charge carriers is fast and fully reversible and they are easy to generate and propagate through space without damaging the plasmonic material. The interaction of a magnetic field with free electrons in nanostructures can be modeled accurately on the basis of Lorentz forces acting on such charge carriers, whose motion is triggered by electric field of light and is then perturbed by the external magnetic field. Such perturbation splits circular plasmonic modes, which can be selectively addressed with light of opposite helicity using magneto-optical techniques. Such techniques take advantage of polarization modulation and phase-sensitive detection to reveal the relatively weak shift (<0.1 meV for noble metals) of plasmonic modes. On the other hand, directly probing field-

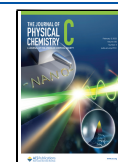
induced shifts using static polarization remains a challenging and yet unexplored goal which would improve the understanding of magnetoplasmonic effects.

Several exciting results have been presented in the past decade, enriching the field of magnetoplasmonics with a wide library of material combinations,¹⁰ ranging from pure noble metals^{11–17} or ferromagnetic metal nanostructures^{18,19} to hybrid multilayered nanostructures made of either noble metals and ferromagnetic moieties.^{20–22} More recently, also plasmonic transparent conductive oxide nanocrystals²³ and nonmagnetic or magnetic hyperbolic nanostructures^{24–26} have been reported to exhibit magnetoplasmonic modulation. Fascinating correlations between localized plasmons and the magneto-optical response at the excitonic resonance have also been reported in doped semiconductor nanocrystals.^{27–29} To date, among homogeneous nanostructures, plasmonic ferro-

Received: November 18, 2021

Revised: January 10, 2022

Published: January 25, 2022



magnetic metal nanostructures exhibit the highest magneto-plasmonic modulation.¹⁹ However, magnetic metals suffer from significant optical losses which decrease the quality factor of their plasmonic resonances, thus limiting their performance for their application in devices. On the other hand, noble metals exhibit higher quality factors due to their reduced losses and sharper resonances. Nevertheless, their modulation is still weak at relatively low magnetic fields (of the order of 1 T).^{11–17} Even if such a response is predicted to linearly increase with the applied magnetic field, ultrahigh magnetic fields are needed to achieve the large magnetoplasmonic response of ferromagnetic nanodisks. Such large fields are hardly achievable with common laboratory-scale equipment, but the experimental analysis of their effect may broaden the understanding of magnetoplasmonic phenomena, thus enabling novel and efficient strategies for future applications. For instance, coupling magnetoplasmonic effects in noble metals to molecular optical transitions can induce enhanced magneto-optical activity in plasmonic–excitonic hybrids^{30,31} or enable detection of magnetic hysteresis of sub-monolayers of single molecule magnets.³² Recently, promising and elegant approaches has been proposed to enhance the magnetoplasmonic response, for instance, by exploiting dark modes in plasmonic nanocavities coupled to magnetic disks³³ or by exploiting surface lattice resonance effects in regularly arranged arrays of plasmonic nanostructures.^{34,35} However, the latter approaches require accurate engineering of the nanostructure array, which is only possible with complex nanofabrication techniques, which limit sample sizes to hundreds of micrometers.

Here we report a thorough investigation of the magneto-plasmonic response of silver nanoparticles films embedded in a silica matrix, prepared by sol–gel synthesis on square centimeter fused silica, employing magnetic circular dichroism (MCD) at different magnetic fields (up to 30 T). Such nanoparticles exhibit an enhanced magneto-optical response with respect to gold nanoparticles (Au NPs) for the same applied field and optical density. An accurate fitting of optical and magneto-optical spectra allows ascribing the enhanced MCD response to the reduced optical losses of silver compared to gold. Moreover, the magneto-optical properties are investigated in a wide magnetic field range reaching extremely high fields up to 30 T, not reachable in in-lab experiments. Our investigation shows a linear field-dependence of the MCD signal up to 30 T, in agreement with the field dependence of the optical properties of metals predicted by the Drude model. For the first time, we demonstrate direct field-induced shift of plasmonic modes using a static circular polarization at 30 T, achieving an excellent agreement with standard magneto-optical spectroscopic techniques based on phase-sensitive detection.

METHODS

Materials. 3-Aminopropyltriethoxysilane (98%) was purchased from ABCR, and silver acetate ($\geq 99.0\%$), ethanol ($\geq 99.8\%$), isopropanol ($\geq 99.7\%$), glacial acetic acid ($\geq 99.7\%$), and concentrated hydrochloric acid (37%) were purchased from Sigma-Aldrich. Fused silica slides were purchased from Haereus. Ultrapure water was obtained from a Milli-Q system (Millipore Corporation).

Synthesis of Silica-Embedded Silver Nanoparticles. Silica-embedded Ag NP samples supported on fused silica slides were prepared using a sol–gel based method.³⁶ Briefly, 6.54 mmol of 3-aminopropyltriethoxysilane, 65.4 mmol of

ethanol, 27.6 mmol of deionized water, and 2.22 mmol of glacial acetic acid were mixed together. The mixture was kept under magnetic stirring for 1 h, and then 0.163 mmol of silver acetate was added (Ag:Si atomic ratio: 0.025); the solution was stirred for 20 h at RT, during which the hydrolysis of the alkoxide took place. Fused silica slides were cleaned by sonication (10 min) in a diluted aqueous solution of household detergent and subsequently rinsed with the following liquid media: 10% HCl aqueous solution, diluted aqueous solution of household detergent, and pure isopropanol. The solution was then cast on the fused silica slides via spin coating (SCS 6800, 2000 rpm, 60 s + 4000 rpm, 60 s) and heat treated in a preheated tubular oven at 800 °C for 60 min. The initially colorless slide turned yellow after the heat treatment.

Au NPs were synthesized by the reduction of HAuCl_4 in organic solvents as previously described.¹³

Morphological and Optical Characterization. *Transmission Electron Microscopy (TEM).* Transmission electron micrographs were acquired on a Tecnai F20 Supertwin field-emission gun microscope working at an accelerating voltage of 200 kV and equipped with an EDAX energy dispersive X-ray spectrometer (EDS) and a high-angle annular dark field (HAADF) detector for scanning TEM imaging. The samples were prepared and measured in cross sections.

Optical Extinction. Optical extinction was measured in transmission geometry with a Jasco V-670 spectrophotometer.

Magnetic Circular Dichroism (MCD). This type of magneto-optical spectroscopy uses circularly polarized (CP) light modulated at high frequency (of the order of 10^4 Hz) between the two opposite helicities, impinging on the sample parallel to the applied magnetic field; the transmitted light thus contains an oscillating component which is proportional to the dichroism and which is recovered via phase-sensitive detection techniques.^{37,38} Such a method allows the detection of dichroic signals (ΔA) of the order of 10^{-6} with respect to the absorption on a well-tuned setup. For both described setups, the following convention was used: the applied field is positive (negative) when parallel (antiparallel) to the light propagation direction, and light is right (left) circularly polarized (RCP and LCP) when the electric field vector rotates clockwise (counterclockwise), observing light from the detector toward the source.

Low Field MCD Setup. Measurements were carried out on a homemade, lab-scale instrument. Light emitted by a 200 W Xe(Hg) arc lamp (Newport Oriel Apex Illuminator) is monochromated (Newport Oriel Cornerstone 130 1/8 m) and chopped at 440 Hz; polarization modulation at 50 kHz between LCP and RCP is obtained with a Glan-Thompson polarizer coupled to a photoelastic modulator (Hinds Instruments PEM 90 I/FSS0) set to $\lambda/4$ retardation. The beam is then directed through the bore of an electromagnet (Buckley Systems Ltd. GMW model 3470) where the sample is placed; light is collected by a photomultiplier tube (Hamamatsu R376). After transimpedance amplification, the voltage is fed to two lock-in amplifiers, one referenced to the polarization modulation frequency (Stanford Research Systems SR850) and one to the light chopping frequency (Princeton Applied Research model 5301); the ratio of the two signals is taken as the differential absorption (dichroism) ΔA . Calibration is carried out against an aqueous solution of $\text{Fe}(\text{CN})_6^{3+}$ of known concentration.

High Field MCD Setup. The instrument has the same optical scheme of the low field setup, but using the following

components: a 100 Xe arc lamp (Lot Oriel), a monochromator (Princeton Instruments Acton SP2300), a photoelastic modulator (Hinds Instruments PEM90), a preamplified silicon photodiode (Thorlabs), and two lock-in amplifiers (Stanford Research Systems SR830). The magnet used in this setup is the 33 T bitter magnet placed in Cell 3 of the High Field Magnet Laboratory of the Radboud University (Nijmegen NL).

High Field CP Absorption. The same convention used in the previous setups was employed for this experiment. The CP absorption measurement was carried out at Cell 3 in HFML laboratory; the optical setup uses the same elements as the one described for MCD measurements, with the exception that CP polarization in this case is static, so the PEM element and its coupled lock-in amplifier are replaced by an achromatic quarter wave plate. Left and right CP light are selected by changing the relative angle between the two polarizing elements from 0° to 180° . The wavevector and the direction of the magnetic field were either parallel or antiparallel, depending of the polarity of the applied field.

RESULTS AND DISCUSSION

Silica-embedded Ag NPs were prepared using a sol–gel method (see [Methods](#) for a detailed description of the synthesis), based on the simultaneous thermal reduction of silver acetate in a silica matrix as the latter is formed from the thermolysis of the precursor alkoxydes.³⁶ The obtained Ag NPs embedded in silica are stable over a long time span, and samples can be cast into high quality films on quartz slides ([Figure 1a](#)). TEM, performed on thin sections of the quartz slides ([Figure 1b](#) and [c](#); [Figure S1](#) in the Supporting Information), shows the presence of highly crystalline NPs (with an average size of 6.9 nm and a standard deviation of 4.7 nm) dispersed into a silica matrix around 500 nm thick. Energy

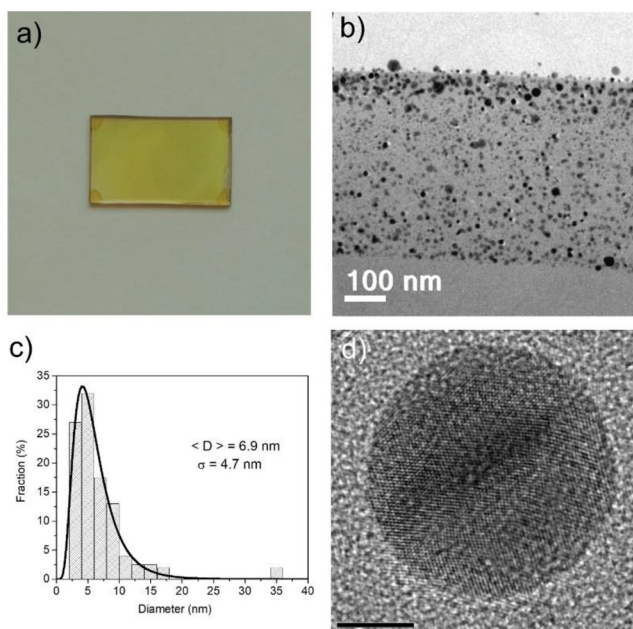


Figure 1. (a) Silica embedded Au NPs casted into high quality films on quartz slides; (b) representative TEM micrograph on a thin section of the quartz slide; (c) size distribution of Ag NPs (the black solid line represents the log-normal fit); (d) detail at high resolution of a nanoparticle of Ag (scale bar: 10 nm).

dispersive X-ray spectra ([Figure S1](#)) revealed an atomic Ag content of 0.8%. High resolution TEM micrographs ([Figure 1d](#)) confirm that the particles are highly crystalline and have an fcc structure with a cell parameter ($a = 4.10 \pm 0.05$ Å) in excellent agreement with that of reference bulk Ag.

To characterize the magnetoplasmonic response of the prepared nanoparticles, we employed room temperature MCD spectroscopy under an applied field of 1.3 T. The obtained spectrum was compared with our previous results on monodisperse Au NPs with similar size and shape, prepared by colloidal chemistry synthesis.¹³ Both Au and Ag NPs show a well-defined localized surface plasmonic resonance (LSPR) centered at ~ 2.38 and ~ 3.05 eV, respectively ([Figure 2a](#)),

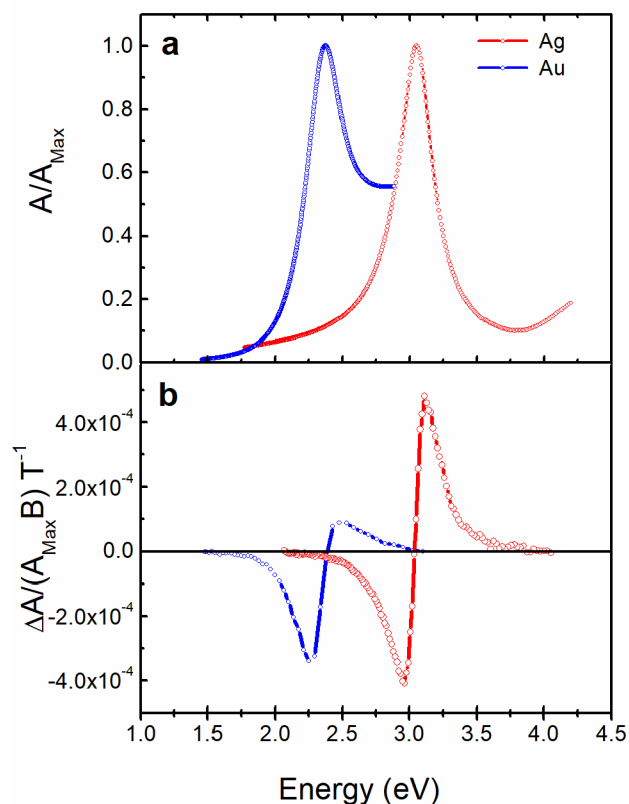


Figure 2. (a) Extinction spectra of Ag (red) and Au (blue) NPs, normalized to the maximum of the plasmonic resonance peak. (b) magnetic circular dichroism spectra of Ag (red) and Au NPs (blue), normalized by the maximum of the absorption peak and by the applied magnetic field.

coherently with the literature data on analogous systems.^{39–41} MCD spectroscopy measures the difference (ΔA) between left-handed and right-handed circularly polarized (LCP and RCP, respectively) light absorption (A) in the presence of a static magnetic field. A derivative-like MCD line shape centered at the extinction maximum is obtained ([Figure 2b](#)) for both Ag and Au spherical NPs, in agreement with previous experimental observations.^{13,14} Such a spectral line shape indicates that light with opposite helicity excites a circular plasmonic mode that is oppositely shifted in energy by an applied field perpendicular to the plane of the plasmonic oscillation, as predicted by the model previously developed for Au NPs, based on Lorentz force evaluation.^{11,13} On the basis of this model, the intensity of the differential signal increases proportionally by increasing the amplitude of the shift, while

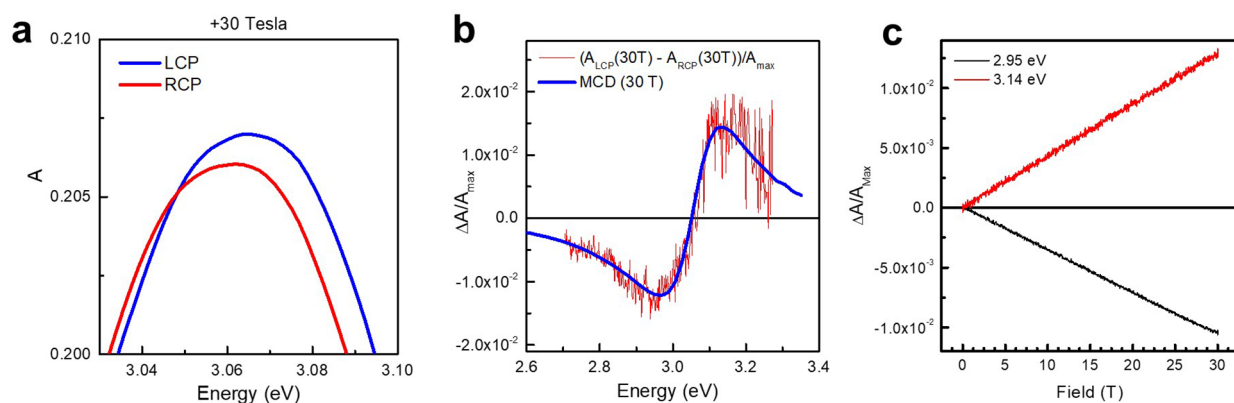


Figure 3. (a) Extinction spectra of Ag NPs collected at 30 T with static circular polarizations of opposite helicities. (b) Comparison between the difference of the two extinction spectra in (a) and the MCD spectrum acquired using the standard polarization-modulation technique. The spectra are normalized at the extinction maximum. (c) Magnetic circular dichroism spectrum of Ag NPs, as a function of the magnetic field between 0 and 30 T measured at fixed wavelengths corresponding to the two lobes.

the line shape is not expected to change in the limit of small shifts compared with peak width.

It is worth noting that, while for spherical Au NPs an asymmetric MCD response is commonly found,^{13,17} in the case of Ag NPs the line shape is symmetric. This difference is ascribed to the electronic properties of the two metals. In the case of gold, the dipolar plasmonic resonance is spectrally overlapped with the interband transition threshold. The presence of such transitions makes the imaginary part of the dielectric function of Au (ϵ'') non-negligible and induces a strong frequency dispersion near the LSPR energy, which causes a difference in intensity of the oppositely shifted plasmonic modes thus resulting in an asymmetry of the MCD line shape.¹¹ However, it has been reported that such asymmetry is completely or partially removed shifting the resonance toward the red spectral region, far from the interband transitions, i.e., coating Au nanospheres with a dielectric material with high permittivity¹⁶ or changing the shape to nanodisks.³² On the other hand, in silver NPs, LSPR and interband transitions are well separated and consequently ϵ'' is small and constant near the resonance energy, yielding a symmetric MCD line shape.

Remarkably, the amplitude of the magneto-optical signal from Ag NPs is more than double with respect to the spectrum measured by the same set up on Au NPs, for the same optical density and applied field. According to our model, the amplitude is directly proportional to the energy shift induced by the magnetic field on the plasmonic resonance. However, another effect contributing to the increase of the signal is the line width of the plasmonic resonance. Indeed, for a given value of the field-induced shift, sharper peaks give a larger MCD signal. In order to discriminate between the two effects, an analytical equation of the field-induced energy shift ($\Delta\omega$) has been derived in previous work from the generalized Fröhlich condition (see the Supporting Information for more details):^{13,16}

$$\Delta\omega = \frac{B\Delta f_1(\omega_0)}{\left. \frac{\partial \epsilon_1}{\partial \omega} \right|_{\omega_0} + B \left. \frac{\partial \Delta f_1}{\partial \omega} \right|_{\omega_0}} \quad (1)$$

where ϵ_1 is the real part of the dielectric function of the metal, ω_0 is the LSPR resonance frequency, and f_1 is the coupling function describing the effect of magnetic field on free

electrons (see the Supporting Information for more detailed information). The quantities $\delta\epsilon_1/\delta\omega$ and $\delta f_1/\delta\omega$ in eq 1 are computed by differentiation with respect to the photon frequency of the dielectric function and the coupling function respectively, and are calculated at the resonant energy ω_0 .

According to this equation, by using the full dielectric function of Au and Ag,⁴² the energy shift at the applied field is only 25% different for the two metals (0.034 meV/T for Au and 0.047 meV/T for Ag), which cannot fully account for the large difference in magneto-optical signal.

In order to get better insight into the magneto-optical properties of Ag NPs, a detailed analysis of the extinction and MCD spectra was performed, considering the MCD signal as the difference of two plasmonic peaks shifted in energy. The optical peak in Ag NPs was deconvolved from the interband transition by using a Lorentz and a Gaussian function respectively (Figure S2 a). The fitting of the MCD spectra (Figure S2b) was performed with a function made by the difference of two Lorentz functions, each one shifted in spectral position by a quantity $\Delta\omega$, neglecting the contribution of interband transitions in the MCD signal in first approximation. In the latter fitting, a rigid shift of the peaks was assumed, thus considering amplitude and width as fixed to the values obtained fitting the extinction spectrum. On the other hand, $\Delta\omega$ representing the splitting between circular magnetoplasmonic modes was left free in the fitting. The fitting model reproduces the experimental spectra of Ag NPs with reasonable agreement (Figure S2), while in Au NPs an additional fitting factor taking into account for changes in intensity of the two shifted peaks is needed, allowing to better reproduce the MCD asymmetry (the analysis is reported in our previous work).¹⁶ A reduced line width was obtained for Ag NPs (0.33 eV instead of 0.41 eV for Au), which can be ascribed to the lower optical losses of silver compared to gold. An increased energy shift is also observed: 0.050 meV instead of 0.034 meV for Au. Remarkably, the obtained shift is in reasonable agreement with the values calculated by applying eq 1. The reduced line width and increased field-induced shift can be identified as the crucial parameters that cause a larger magnetoplasmonic response for Ag NPs.

The linear dependence of the magnetic field-induced splitting of circular plasmonic modes in our model is a consequence of a low-field approximation, which has been

confirmed to be valid for laboratory scale magnetic field values.¹³ However, to date, no report has appeared on experiments carried out under extremely intense magnetic fields available at large scale facilities. Thus, we performed a MCD experiment under these conditions ($\mu_0H = 30$ T) to test the validity of the linear model.

The comparison of MCD spectrum of Ag NPs at 30 T (Figure 3) with the low magnetic field effect (Figure S 3) clearly indicates that the MCD line shape does not depend on the μ_0H intensity and the two spectra normalized for the magnitude of the applied magnetic field are superimposable. This confirms the hypothesis that the field-induced shift is rigid, without detectable changes in the plasmonic broadening.

Aiming at directly observing the field-induced shift of individual circular plasmonic modes, we performed absorption experiments with static circular polarizations at 30 T, instead of modulating the polarization and directly acquiring the differential absorption signal as commonly performed in magneto-optical spectroscopies. Remarkably, the shift is clearly visible in the separated absorption spectra acquired with RCP and LCP at 30 T (Figure 3a). The two shifted peaks collected with RCP and LCP have comparable full widths at half-maximum, as confirmed by the larger view of the two spectra reported in Figure S4, which implies that the two magneto-plasmonic modes have comparable dephasing time or at least their difference in line width (predicted by Weick and Weinmann⁴³) is not detectable, as it is much lower compared to the main cause of plasmon broadening, such as surface electron-scattering. Moreover, the difference between the two spectra gives an MCD spectrum (Figure 3b) which, despite significant noise, is superimposable with the one acquired using the standard MCD technique (exploiting phase-sensitive detection). We should point out that the noise in the curve obtained from the difference between the two CP absorptions is largely expected due to the extreme difficulty in detecting very small differences in absorption without polarization modulation, which is here possible to distinguish only due to the high magnetic field applied. A similar result, but with an opposite sign of the obtained MCD spectrum, is observed applying a negative field of -30 T (Figure S5).

As predicted by our model, the amplitude of the MCD signal at 3.14 and 2.95 eV (corresponding to the positive and the negative lobes respectively) exhibits a completely linear field dependence (Figure 3c) up to very high magnetic fields (0–30 T), while the residual between experimental and simulated scans is well below the experimental error on the MCD measurement (not shown). It is thus confirmed that the magneto-plasmonic response is linear up to very high magnetic fields, denoting that the magnetic cyclotron effect can be treated as perturbation of the plasmonic resonance up to extreme values of H .

CONCLUSIONS

We measured the magnetic-field-induced circular dichroism in silver NPs up to a very high magnetic field (30 T). The MCD signal in silver is 2-fold enhanced with respect to colloidal gold NPs. We show that the enhancement is mainly due to the reduced plasmon losses in Ag with respect to Au, ascribed to the wider separation between LSPR and interband transitions in silver. Through extinction spectroscopy with static circular polarization (RCP and LCP) at 30 T, we were able to directly detect for the first time the splitting between the two circular magneto-plasmonic modes without the need of modulating the

polarization of light. We finally demonstrate that the magneto-plasmonic effect is linear with the magnetic field up to 30 T, thus validating the rigid cyclotron shift model for large fields.

Given the recent interest in magneto-plasmonics effects in novel plasmonic materials, such as doped semiconductors²³ and hyperbolic nanomaterials,²⁴ our results are expected to provide useful tools in view of the application of magneto-plasmonic effects: on the experimental side by demonstrating the possibility to achieve large magnetic modulation even in nonmagnetic nanomaterials by applying very high magnetic fields; on the theoretical side, the importance of reducing optical losses to enlarge magneto-plasmonic effects is further affirmed by our investigation.

ASSOCIATED CONTENT

Supporting Information

The Supporting Information is available free of charge at <https://pubs.acs.org/doi/10.1021/acs.jpcc.1c09900>.

HAADF and EDS spectra of Ag NPs; fitting of extinction and MCD spectra, comparison between high field and low field MCD of Ag NPs; large view of the spectra obtained and static RCP (LCP) light and 30 T of applied field; high field MCD obtained by subtracting extinction spectra obtained with RCP and LCP, with +30 and -30 T; details of the analytical model to simulate the MCD response and the field-induced energy shift of the plasmonic resonance (PDF)

AUTHOR INFORMATION

Corresponding Author

Francesco Pineider – *INSTM and Department of Chemistry and Industrial Chemistry, University of Pisa, 56124 Pisa, Italy; Department of Physics and Astronomy, University of Florence, 50019 Sesto Fiorentino (FI), Italy; orcid.org/0000-0003-4066-4031; Email: francesco.pineider@unipi.it*

Authors

Alessio Gabbani – *INSTM and Department of Chemistry and Industrial Chemistry, University of Pisa, 56124 Pisa, Italy; CNR-ICCOM, 50019 Sesto Fiorentino (FI), Italy; Department of Physics and Astronomy, University of Florence, 50019 Sesto Fiorentino (FI), Italy; orcid.org/0000-0002-4078-0254*

Giulio Campo – *INSTM and Department of Chemistry, University of Florence, 50019 Sesto Fiorentino (FI), Italy; orcid.org/0000-0003-3777-4520*

Valentina Bonanni – *INSTM and Department of Chemistry, University of Florence, 50019 Sesto Fiorentino (FI), Italy; Elettra-Sincrotrone Trieste, 34149 Trieste, Italy; orcid.org/0000-0001-8346-0069*

Peter van Rhee – *High Field Magnet Laboratory (HFML - EMFL), Radboud University, 6525 ED Nijmegen, The Netherlands*

Gregorio Bottaro – *Istituto di Chimica della Materia Condensata e di Tecnologie per l'Energia, Consiglio Nazionale delle Ricerche, ICMATE-CNR, Università di Padova, I 35131 Padova, Italy; INSTM and Dipartimento di Scienze Chimiche, Università di Padova, I 35131 Padova, Italy; orcid.org/0000-0001-6196-8638*

César de Julián Fernández – *IMEM-CNR, 43124 Parma, Italy; orcid.org/0000-0002-6671-2743*

Valentina Bello – Department of Physics, University of Padova, 35121 Padova, Italy
Elvira Fantechi – INSTM and Department of Chemistry and Industrial Chemistry, University of Pisa, 56124 Pisa, Italy; orcid.org/0000-0002-9323-2198
Francesco Biccari – Department of Physics and Astronomy, University of Florence, 50019 Sesto Fiorentino (FI), Italy
Massimo Gurioli – Department of Physics and Astronomy, University of Florence, 50019 Sesto Fiorentino (FI), Italy; orcid.org/0000-0002-6779-1041
Lidia Armelao – INSTM and Dipartimento di Scienze Chimiche, Università di Padova, I 35131 Padova, Italy; Dipartimento di Scienze Chimiche e Tecnologie dei Materiali (DSCTM), Consiglio-Nazionale delle Ricerche, 00185 Roma, Italy
Claudio Sangregorio – CNR-ICCOM, 50019 Sesto Fiorentino (FI), Italy; orcid.org/0000-0002-2655-3901
Giovanni Mattei – Department of Physics, University of Padova, 35121 Padova, Italy
Peter Christianen – High Field Magnet Laboratory (HFML - EMFL), Radboud University, 6525 ED Nijmegen, The Netherlands

Complete contact information is available at:
<https://pubs.acs.org/10.1021/acs.jpcc.1c09900>

Author Contributions

The manuscript was written through contributions of all authors. All authors have given approval to the final version of the manuscript.

Notes

The authors declare no competing financial interest.

ACKNOWLEDGMENTS

This work was supported by HFML-RU/NWO-I, member of the European Magnetic Field Laboratory (EMFL). F.P., A.G., and E.F. acknowledge the financial support of PRIN2017 under Grant No. 2017CR5WCH Q-ChiSS (Italian MIUR) and of PRA_2017_25 (Università di Pisa).

REFERENCES

- (1) Jiang, N.; Zhuo, X.; Wang, J. Active Plasmonics: Principles, Structures, and Applications. *Chem. Rev.* **2018**, *118*, 3054.
- (2) Krasnok, A.; Alù, A. Active Nanophotonics. *Proceedings of the IEEE* **2020**, *108* (5), 628–654.
- (3) Maccaferri, N.; Zubritskaya, I.; Rzdolski, I.; Chioar, I.-A.; Belotelov, V.; Kapaklis, V.; Oppeneer, P. M.; Dmitriev, A. Nanoscale Magnetophotonics. *J. Appl. Phys.* **2020**, *127* (8), 080903.
- (4) MacDonald, K. F.; Sámson, Z. L.; Stockman, M. I.; Zheludev, N. I. Ultrafast Active Plasmonics. *Nat. Photonics* **2009**, *3* (1), 55–58.
- (5) Pacifici, D.; Lezec, H. J.; Atwater, H. A. All-Optical Modulation by Plasmonic Excitation of CdSe Quantum Dots. *Nat. Photonics* **2007**, *1* (7), 402–406.
- (6) Taghinejad, M.; Taghinejad, H.; Xu, Z.; Liu, Y.; Rodrigues, S. P.; Lee, K.-T.; Lian, T.; Adibi, A.; Cai, W. Hot-Electron-Assisted Femtosecond All-Optical Modulation in Plasmonics. *Adv. Mater.* **2018**, *30* (9), 1704915.
- (7) Michel, A.-K. U.; Chigrin, D. N.; Maß, T. W. W.; Schönauer, K.; Salinga, M.; Wuttig, M.; Taubner, T. Using Low-Loss Phase-Change Materials for Mid-Infrared Antenna Resonance Tuning. *Nano Lett.* **2013**, *13* (8), 3470–3475.
- (8) Chang, W.-S.; Lassiter, J. B.; Swanglap, P.; Sobhani, H.; Khatua, S.; Nordlander, P.; Halas, N. J.; Link, S. A Plasmonic Fano Switch. *Nano Lett.* **2012**, *12* (9), 4977–4982.
- (9) Llordés, A.; Garcia, G.; Gazquez, J.; Milliron, D. J. Tunable Near-Infrared and Visible-Light Transmittance in Nanocrystal-in-Glass Composites. *Nature* **2013**, *500* (7462), 323–326.
- (10) de Julián Fernández, C.; Pineider, F. Magneto-Plasmonic Nanoparticles. In *New Trends in Nanoparticle Magnetism*; Peddis, D., Laureti, S., Fiorani, D., Eds.; Springer Series in Materials Science; Springer International Publishing: Cham, 2021; pp 107–136.
- (11) Gabbani, A.; Petrucci, G.; Pineider, F. Magneto-Optical Methods for Magnetoplasmonics in Noble Metal Nanostructures. *J. Appl. Phys.* **2021**, *129* (21), 211101.
- (12) Sepúlveda, B.; González-Díaz, J. B.; García-Martín, A.; Lechuga, L. M.; Armelles, G. Plasmon-Induced Magneto-Optical Activity in Nanosized Gold Disks. *Phys. Rev. Lett.* **2010**, *104* (14), 147401.
- (13) Pineider, F.; Campo, G.; Bonanni, V.; de Julián Fernández, C.; Mattei, G.; Caneschi, A.; Gatteschi, D.; Sangregorio, C. Circular Magnetoplasmonic Modes in Gold Nanoparticles. *Nano Lett.* **2013**, *13* (10), 4785–4789.
- (14) Shiratsu, T.; Yao, H. Size Dependence of Magneto-Optical Activity in Silver Nanoparticles with Dimensions between 10 and 60 Nm Studied by MCD Spectroscopy. *Phys. Chem. Chem. Phys.* **2018**, *20* (6), 4269–4276.
- (15) Nagumo, Y.; Yao, H. Magnetic Circular Dichroism Responses with High Sensitivity and Enhanced Spectral Resolution in Multipolar Plasmonic Modes of Silver Nanoparticles with Dimensions between 90 and 200 Nm. *J. Phys. Chem. Lett.* **2021**, *12* (38), 9377–9383.
- (16) Gabbani, A.; Fantechi, E.; Petrucci, G.; Campo, G.; de Julián Fernández, C.; Ghigna, P.; Sorace, L.; Bonanni, V.; Gurioli, M.; Sangregorio, C.; et al. Dielectric Effects in FeO_x-Coated Au Nanoparticles Boost the Magnetoplasmonic Response: Implications for Active Plasmonic Devices. *ACS Appl. Nano Mater.* **2021**, *4*, 1057.
- (17) Han, B.; Gao, X.; Lv, J.; Tang, Z. Magnetic Circular Dichroism in Nanomaterials: New Opportunity in Understanding and Modulation of Excitonic and Plasmonic Resonances. *Adv. Mater.* **2020**, *32*, 1801491.
- (18) Bonanni, V.; Bonetti, S.; Pakizeh, T.; Pirzadeh, Z.; Chen, J.; Nogués, J.; Vavassori, P.; Hillenbrand, R.; Åkerman, J.; Dmitriev, A. Designer Magnetoplasmonics with Nickel Nanoferrromagnets. *Nano Lett.* **2011**, *11* (12), 5333–5338.
- (19) Maccaferri, N.; E. Gregorczyk, K.; de Oliveira, T. V. A. G.; Kataja, M.; van Dijken, S.; Pirzadeh, Z.; Dmitriev, A.; Åkerman, J.; Knez, M.; Vavassori, P. Ultrasensitive and Label-Free Molecular-Level Detection Enabled by Light Phase Control in Magnetoplasmonic Nanoantennas. *Nat. Commun.* **2015**, *6*, 6150.
- (20) Armelles, G.; Caballero, B.; Cebollada, A.; Garcia-Martin, A.; Meneses-Rodríguez, D. Magnetic Field Modification of Optical Magnetic Dipoles. *Nano Lett.* **2015**, *15* (3), 2045–2049.
- (21) Belotelov, V. I.; Akimov, I. A.; Pohl, M.; Kotov, V. A.; Kasture, S.; Vengurlekar, A. S.; Gopal, A. V.; Yakovlev, D. R.; Zvezdin, A. K.; Bayer, M. Enhanced Magneto-Optical Effects in Magnetoplasmonic Crystals. *Nat. Nanotechnol.* **2011**, *6* (6), 370–376.
- (22) Temnov, V. V.; Armelles, G.; Woggon, U.; Guzatov, D.; Cebollada, A.; Garcia-Martin, A.; Garcia-Martin, J.-M.; Thomay, T.; Leitenstorfer, A.; Bratschitsch, R. Active Magneto-Plasmonics in Hybrid Metal–Ferromagnet Structures. *Nat. Photonics* **2010**, *4* (2), 107–111.
- (23) Gabbani, A.; Sangregorio, C.; Tandon, B.; Nag, A.; Gurioli, M.; Pineider, F. Active Magnetoplasmonics with Transparent Conductive Oxide Nanocrystals. *arXiv (Optics)*, April 15, **2021**, 2104.07772, ver. 1.
- (24) Kuttruff, J.; Gabbani, A.; Petrucci, G.; Zhao, Y.; Iarossi, M.; Pedrueza-Villalmanzo, E.; Dmitriev, A.; Parracino, A.; Strangi, G.; De Angelis, F.; et al. Magneto-Optical Activity in Nonmagnetic Hyperbolic Nanoparticles. *Phys. Rev. Lett.* **2021**, *127* (21), 217402.
- (25) Wang, X.; Wang, H.; Jian, J.; Rutherford, B. X.; Gao, X.; Xu, X.; Zhang, X.; Wang, H. Metal-Free Oxide-Nitride Heterostructure as a Tunable Hyperbolic Metamaterial Platform. *Nano Lett.* **2020**, *20* (9), 6614–6622.

(26) Kolmychek, I. A.; Pomozov, A. R.; Leontiev, A. P.; Napolskii, K. S.; Murzina, T. V. Magneto-Optical Effects in Hyperbolic Metamaterials. *Opt. Lett.*, **OL** **2018**, *43* (16), 3917–3920.

(27) Yin, P.; Tan, Y.; Fang, H.; Hegde, M.; Radovanovic, P. V. Plasmon-Induced Carrier Polarization in Semiconductor Nanocrystals. *Nat. Nanotechnol.* **2018**, *13* (6), 463–467.

(28) Yin, P.; Tan, Y.; Ward, M. J.; Hegde, M.; Radovanovic, P. V. Effect of Dopant Activation and Plasmon Damping on Carrier Polarization in In_2O_3 Nanocrystals. *J. Phys. Chem. C* **2019**, *123* (49), 29829–29837.

(29) Yin, P.; Hegde, M.; Tan, Y.; Chen, S.; Garnet, N.; Radovanovic, P. V. Controlling the Mechanism of Excitonic Splitting in In_2O_3 Nanocrystals by Carrier Delocalization. *ACS Nano* **2018**, *12* (11), 11211–11218.

(30) Melnikau, D.; Govyadinov, A. A.; Sánchez-Iglesias, A.; Grzelczak, M.; Nabiev, I. R.; Liz-Marzán, L. M.; Rakovich, Y. P. Double Rabi Splitting in a Strongly Coupled System of Core–Shell $\text{Au}@\text{Ag}$ Nanorods and J-Aggregates of Multiple Fluorophores. *J. Phys. Chem. Lett.* **2019**, *10* (20), 6137–6143.

(31) Melnikau, D.; Govyadinov, A. A.; Sánchez-Iglesias, A.; Grzelczak, M.; Liz-Marzán, L. M.; Rakovich, Y. P. Strong Magneto-Optical Response of Nonmagnetic Organic Materials Coupled to Plasmonic Nanostructures. *Nano Lett.* **2017**, *17* (3), 1808–1813.

(32) Pineider, F.; Pedrueza-Villalmanzo, E.; Serri, M.; Adamo, A. M.; Smetanina, E.; Bonanni, V.; Campo, G.; Poggini, L.; Mannini, M.; Fernández, C.; et al. Plasmon-Enhanced Magneto-Optical Detection of Single-Molecule Magnets. *Mater. Horiz.* **2019**, *6* (6), 1148–1155.

(33) López-Ortega, A.; Zapata-Herrera, M.; Maccaferri, N.; Pancaldi, M.; Garcia, M.; Chuvilin, A.; Vavassori, P. Enhanced Magnetic Modulation of Light Polarization Exploiting Hybridization with Multipolar Dark Plasmons in Magnetoplasmonic Nanocavities. *Light Sci. Appl.* **2020**, *9* (49), 1–14.

(34) Kataja, M.; Hakala, T. K.; Julku, A.; Huttunen, M. J.; van Dijken, S.; Törmä, P. Surface Lattice Resonances and Magneto-Optical Response in Magnetic Nanoparticle Arrays. *Nat. Commun.* **2015**, *6* (1), 1–8.

(35) Pourjamal, S.; Kataja, M.; Maccaferri, N.; Vavassori, P.; Van Dijken, S. Hybrid $\text{Ni}/\text{SiO}_2/\text{Au}$ Dimer Arrays for High-Resolution Refractive Index Sensing. *Nanophotonics* **2018**, *7* (5), 905–912.

(36) Armelao, L.; Bertocello, R.; De Dominicis, M. Silver Nanocluster Formation in Silica Coatings by the Sol-Gel Route. *Adv. Mater.* **1997**, *9* (9), 736–741.

(37) Mason, W. R. Spectrometer for Simultaneous Measurement of Absorption and Circular Dichroism Spectra. *Anal. Chem.* **1982**, *54* (4), 646–648.

(38) Mason, W. R. *A Practical Guide to Magnetic Circular Dichroism Spectroscopy*; Wiley-Interscience: Hoboken, NJ, 2007; pp 36–45.

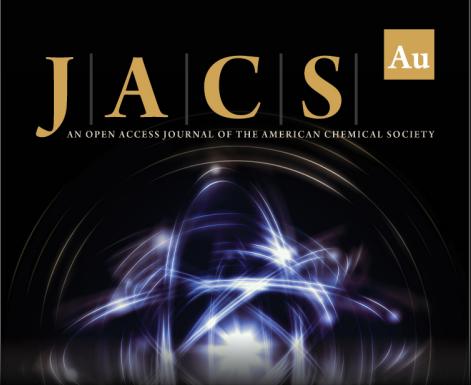
(39) Bastús, N. G.; Merkoçi, F.; Piella, J.; Puentes, V. Synthesis of Highly Monodisperse Citrate-Stabilized Silver Nanoparticles of up to 200 Nm: Kinetic Control and Catalytic Properties. *Chem. Mater.* **2014**, *26* (9), 2836–2846.

(40) Hiramatsu, H.; Osterloh, F. E. A Simple Large-Scale Synthesis of Nearly Monodisperse Gold and Silver Nanoparticles with Adjustable Sizes and with Exchangeable Surfactants. *Chem. Mater.* **2004**, *16* (13), 2509–2511.

(41) Bastús, N. G.; Comenge, J.; Puentes, V. Kinetically Controlled Seeded Growth Synthesis of Citrate-Stabilized Gold Nanoparticles of up to 200 Nm: Size Focusing versus Ostwald Ripening. *Langmuir* **2011**, *27* (17), 11098–11105.


(42) Johnson, P. B.; Christy, R.-W. Optical Constants of the Noble Metals. *Phys. Rev. B* **1972**, *6* (12), 4370.


(43) Weick, G.; Weinmann, D. Lifetime of the Surface Magneto-plasmons in Metallic Nanoparticles. *Phys. Rev. B* **2011**, *83* (12), 125405.



JACS Au
AN OPEN ACCESS JOURNAL OF THE AMERICAN CHEMICAL SOCIETY

Editor-in-Chief
Prof. Christopher W. Jones
Georgia Institute of Technology, USA

Open for Submissions 

pubs.acs.org/jacsau  ACS Publications
Most Trusted. Most Cited. Most Read.